

Electrical impedance-based crack detection of SFRC under varying environmental conditions

Man-Sung Kang^{1a}, Yun-Kyu An^{*1} and Dong-Joo Kim^{2b}

¹Department of Architectural Engineering, Sejong University, 209, Neungdong-ro, Gwangjin-gu, Seoul, 05006, Republic of Korea

²Department of Civil and Environmental Engineering, Sejong University, 209, Neungdong-ro, Gwangjin-gu, Seoul, 05006, Republic of Korea

(Received March 19, 2018, Revised May 10, 2018, Accepted May 24, 2018)

Abstract. This study presents early crack detection of steel fiber-reinforced concrete (SFRC) under varying temperature and humidity conditions using an instantaneous electrical impedance acquisition system. SFRC has the self-sensing capability of electrical impedance without sensor installation thanks to the conductivity of embedded steel fibers, making it possible to effectively monitor cracks initiated in SFRC. However, the electrical impedance is often sensitively changed by environmental effects such as temperature and humidity variations. Thus, the extraction of only crack-induced feature from the measured impedance responses is a crucial issue for the purpose of structural health monitoring. In this study, the instantaneous electrical impedance acquisition system incorporated with SFRC is developed. Then, temperature, humidity and crack initiation effects on the impedance responses are experimentally investigated. Based on the impedance signal pattern observation, it is turned out that the temperature effect is more predominant than the crack initiation and humidity effects. Various crack steps are generated through bending tests, and the corresponding impedance damage indices are extracted by compensating the dominant temperature effect. The test results reveal that propagated cracks as well as early cracks are successfully detected under temperature and humidity variations.

Keywords: self-sensing concrete; electrical impedance; crack detection; steel fiber-reinforced concrete; structural health monitoring; temperature and humidity variation

1. Introduction

A number of historical collapse accidents of civil infrastructures especially made of concrete materials have been reported (Arslan and Korkmaz 2007, Robin 2013). Such accidents are directly connected to civilians' live and property. Thus, their prevention and prediction are one of the most important issues in structural health monitoring (SHM) field. In this perspective, early damage detection from an initial stage is necessary. Although there are many types of concrete damage such as carbonation, delamination, aggregate expansion and so on, a crack is well-known and one of the critical damage types in concrete structures. However, early crack detection of concrete structures is still a challenging work due to inhomogeneity, bulky frame, inherent damage of non-structure level and so on. Visual inspection by well-trained experts has been most widely used in the field, but it is quite labor-intensive, time consuming and unreliable. Thus, a number of ongoing

efforts to develop effective crack detection techniques in concrete structures has been reported. For example, Neild *et al.* (2005) and Simon *et al.* (2015) utilized vibrating wire strain gauges for measuring small strain in concrete. Then, acoustic or ultrasonic sensor-based crack detection techniques have been also proposed. Fiber optic sensors were utilized to monitor acoustic emission in civil structures (Verstrynge *et al.* 2014, Kazuro *et al.* 2005). Then, a lead zirconate titanate (PZT) impedance sensor-based concrete damage detection techniques have been developed (Yanowen *et al.* 2008, Wang *et al.* 2013, Karayannis *et al.* 2015, Arun and Subramaniam 2016.). Suraj and Shruti (2016) and Chalioris *et al.* (2015) also proposed PZT-based smart aggregates for damage evaluation in a concrete beam. Also, wireless impedance monitoring systems has been developed for damage detection concrete beams (Providakis and Liarakos 2011, Chalioris *et al.* 2016, Yan *et al.* 2017). Although they have high detectability to cracks, inhomogeneity of concrete makes the responses difficult to be physically interpreted. Then, the high damping nature of acoustic or ultrasonic waves propagating along concrete structures often degrades crack detectability in terms of low signal-to-noise ratio. Moreover, the sensor installation still has technical problems such as imperfect bonding condition, replacement issues and so on. In particular, the critical issue is that the degradation of embedded sensors is often faster than the target structure when it comes to long-term SHM perspective (An *et al.* 2014).

*Corresponding author, Professor
E-mail: yunkyuan@sejong.ac.kr

^aMS Student
E-mail: kms102353@sju.ac.kr

^bProfessor
E-mail: djkim72@sejong.ac.kr

To overcome the limitations of the contact-type SHM techniques, non-contact SHM techniques have been developed. Vision cameras have been used for concrete crack inspection (Lecompte *et al.* 2006, Jahanshahi *et al.* 2013). Although the vision camera techniques are simple, cost-effective and practical, their reliability may be degraded depending on the image capture conditions such as capture angle, illuminance, undesired dust in the air or on the target surface. Another promising SHM technique is an infrared (IR) thermography technique (Yang *et al.* 2016, An *et al.* 2014, Cheng *et al.* 2008, Aggelis *et al.* 2010). It is also noncontact, nondestructive and non-invasive technique, but the precise control and high-power of an excitation heat source are typically required for concrete crack detection. Furthermore, surface irregularity of concrete structure is often misclassified as a crack due to high sensitivity.

As an alternative, self-sensing concrete materials have been developed. Although concrete is a representative non-conductive material, it is able to have electrical conductivity by adding various conductive functional components such as steel fiber, carbon black, carbon nanofiber, graphite powder and so on, enabling to measure electrical responses without sensor installation (Hou and Lynch 2005, Luo *et al.* 2011, Vaidya and Allouche 2011, Azhari and Banthia 2012, Konsta-Gdoutos and Aza 2014, Qiao *et al.* 2017). In order to measure electrical responses, an electrical input source is required. Direct current (DC) and alternating current (AC) have been used as typical input source types. Although the DC method is simple and stable, relatively long stabilization time caused by polarization effect is typically necessary for the stable response measurement (Jingyao and Chung 2004). Thus, the DC method may not be suitable to instantaneously measure the data for SHM. On the other hand, the AC method can be used for the real-time SHM purpose, because the polarization effect can be eliminated (Baoguo *et al.* 2012). The self-sensing concrete-based AC methods have widely used to measure mechanical behaviors (Xuli *et al.* 1997, Xu *et al.* 2010, Teomete 2015). However, a few studies on the performance of the self-sensing concrete under varying environmental conditions have been reported for the SHM purpose.

In this study, a steel fiber-reinforced concrete (SFRC) based self-sensing electrical impedance technique is proposed for early crack detection. Thanks to the high strength and ductility of SFRC (Jianming *et al.* 1997, Yoo *et al.* 2015, Bae *et al.* 2018), it can be used as structural members in the structural hot spots of a concrete structure. Simultaneously, SFRC is able to act as sensors for SHM, thus making it possible to effectively monitor the entire concrete structure. However, since electrical impedance is sensitively altered by environmental variation as well as crack initiation, a crack-induced feature should be extracted from the measured responses under normal operating or environmental conditions. The objectives of this study are (1) to develop a SFRC-based self-sensing impedance acquisition system for instantaneous data measurement, (2) to experimentally investigate the temperature, humidity and crack initiation effects on the electrical impedance responses obtained using the developed system, and (3) to identify crack initiation in SFRC under environmental

variation.

This paper is organized as follows. Section 2 describes the instantaneous electrical impedance acquisition system combining with SFRC. Then, Section 3 investigates temperature, humidity and crack initiation effects on the measured impedance responses. Based on the signal pattern analysis, the crack detection procedure and the processing results are presented in Section 4. Finally, this paper is concluded with brief discussion in Section 5.

2. Development of an instantaneous electrical impedance acquisition system

This section introduces the SFRC-based electrical impedance acquisition system. First, the manufacturing process of SFRC is explained. Based on the prepared SFRC, an instantaneous electrical impedance acquisition system enabling to excite an AC input with various frequencies and to simultaneously measure the corresponding impedance is developed.

2.1 Preparation of steel fiber-reinforced concrete (SFRC)

SFRC is basically made by adding steel fibers to a mortar matrix, making it possible to have conductive nature. The mortar matrix is basically composed of type I cement, silica fume, silica powder, superplasticizer and water as summarized in Table 1. Here, individual grains of each component are ranged from 0.1 mm to 0.3 mm, and the averaged diameter of silica sand is 0.42 mm.

First, all components are dry-mixed for two minutes, and water is subsequently added. Then, the superplasticizer is additionally mixed during two or three minutes. The resultant strength of the mortar matrix without fiber is 180 MPa. Here, a Hobart type laboratory mixer with a capacity of 20 L is used for mortar mixing. Next, the medium fibers with smooth surface are added to the matrix. For the uniform distribution of fibers, a small of fibers is sequentially added on several times. Similarly, the long smooth fibers are added to the matrix. The portion of the steel fibers is 2 % of the matrix, and their total weight is 93 g. The material property of the steel fibers is shown in Table 2.

Subsequently, the mixtures cast in a mold. Copper electrodes and steel wire meshes are embedded as shown in Fig. 1. The steel wire meshes used for reinforcement are disconnected where the crack will be produced, meaning that the crack initiation location is controlled using the wire mesh installation.

Table 1 Composition of matrix mixture presented by weight ratio

Cement (Type)	Silica fume	Silica sand	Silica powder	Super-plasticizer	Water
1.0 (I)	0.25	1.1	0.3	0.067	0.2

Table 2 Material property of steel fibers

Fiber type	Diameter (mm)	Length (mm)	Density (g/cc)	Tensile strength (MPa)	Elastic modulus (GPa)	Electrical resistivity (k Ω -cm)	Volume contents (%)
Long smooth	0.3	30	7.9	2000	200	2.06×10^{-8}	1.0
Medium smooth	0.2	19	7.9	2788	200	2.06×10^{-8}	1.0

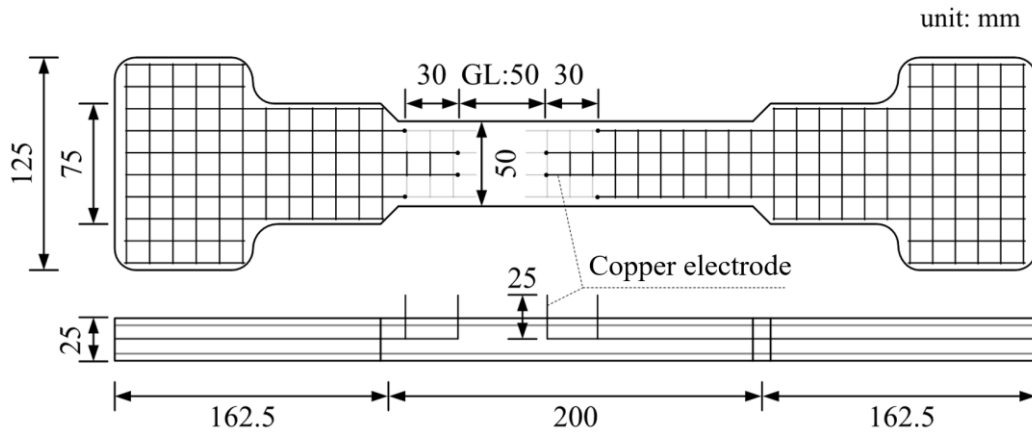


Fig. 1 Dimension of the SFRC specimen

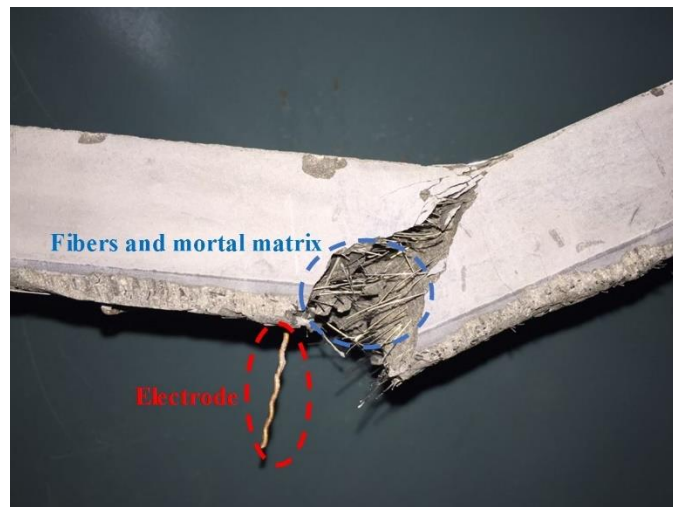


Fig. 2 Representative SFRC specimen fractured by bending loads

Then, the electrical conductivity of the embedded two copper electrodes is 9.21×10^8 /k Ω -cm. Note that the electrode type and material should be carefully selected to enhance the sensing sensitivity. The detailed dimension of the SFRC specimen is shown in Fig. 1.

After the casting process, the SFRC is covered with plastic sheets and placed in laboratory at room temperature of 25 °C and a relative humidity of 60 % for one or two days prior to demolding. Finally, after demolding, SFRC is hot-water-cured at a temperature of 90 °C for three days.

Fig. 2 shows the manufactured SFRC including fibers and electrodes. Note that the fractured one is shown in Fig. 2 so that inner fibers can be simultaneously displayed.

2.2 Instantaneous electrical impedance acquisition system

Fig. 3 shows the electrical impedance acquisition system combined with SFRC. The electrical impedance acquisition system consists of an arbitrary waveform generator (AWG),

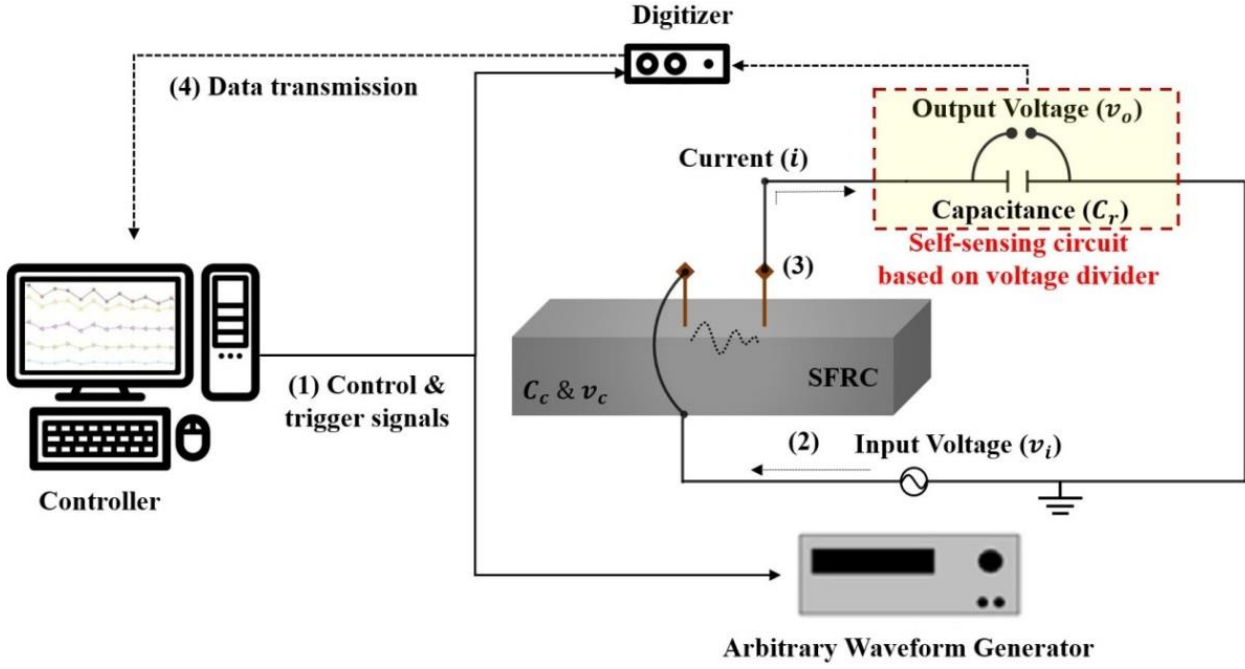


Fig. 3 Schematic of an instantaneous electrical impedance acquisition system: arbitrary waveform generator. v_i , v_o and v_c are input, output and SFRC voltages, respectively. C_c and C_r denote the capacitance values of SFRC and the reference capacitor of the self-sensing circuit

a voltage divider-based self-sensing circuit, a digitizer and a controller. First, the controller sends the control and trigger signals to AWG and digitizer. Then, AWG generates an AC input with a desired waveform, and the corresponding current propagates along SFRC as shown in Fig. 3. Simultaneously, the current is measured by the digitizer through the self-sensing circuit. Since SFRC is semi-conductive, the driving voltage above a certain level is required. However, the closed loop circuit of series connection may cause the saturation of digitizer. Therefore, a self-sensing circuit acting as a charge amplifier is used to measure small voltage of SFRC (An and Sohn 2012). The self-sensing circuit based on a voltage divider is able to simply measure the voltage of SFRC (v_c) using the following equation.

$$v_c(t) = -\frac{C_r}{C_c} v_o(t) - v_i(t) \quad (1)$$

where C_c and C_r represent the capacitance values of SFRC and the reference capacitor of the self-sensing circuit, respectively. v_o and v_i are the voltages of output and input as shown in Fig. 3. And the electrical contacts with the specimen is easily contacted using a crocodile clip. The developed impedance acquisition system is able to automatically sweep broadband frequency ranges, which is programmed by LabVIEW. Note that developed system can be easily extended to multi-channel sensing using multiplexers, although Fig. 3 display the single-channel data acquisition.

3. Experimental study

Based on the developed instantaneous electrical impedance acquisition system, environmental variation and bending load tests are carried out. In particular, the electrical impedance signal patterns are observed under changing operation temperature and humidity conditions. Then, bending-induced crack effects on the impedance signals are also investigated.

3.1 Investigation of temperature and humidity variation effects

The test setup for investigating temperature and humidity variation effects on the impedance signals is shown in Fig. 4. AWG (NI PXI-5412) generates the input waveform of broadband frequency ranged from 65 Hz to 85 Hz, and the digitizer (NI PXI-5122) measures the corresponding responses with a sampling rate of 1MHz. To reduce undesired noises, the responses are 10 times measured and averaged in the time domain for each condition. The reference capacitor of 10 nF is used for the self-sensing circuit, and the measured responses are calibrated using Eq. (1). For the temperature and humidity conditions, the temperature data sets are collected from intact condition of the specimen at -10°C , 0°C , 10°C , 20°C , 30°C and 40°C with a relative humidity 60%. Similarly, the humidity data sets are collected at 40%, 60% and 80% under 20°C . Note that common operating environmental conditions are considered. The test cases are summarized in Table 3.

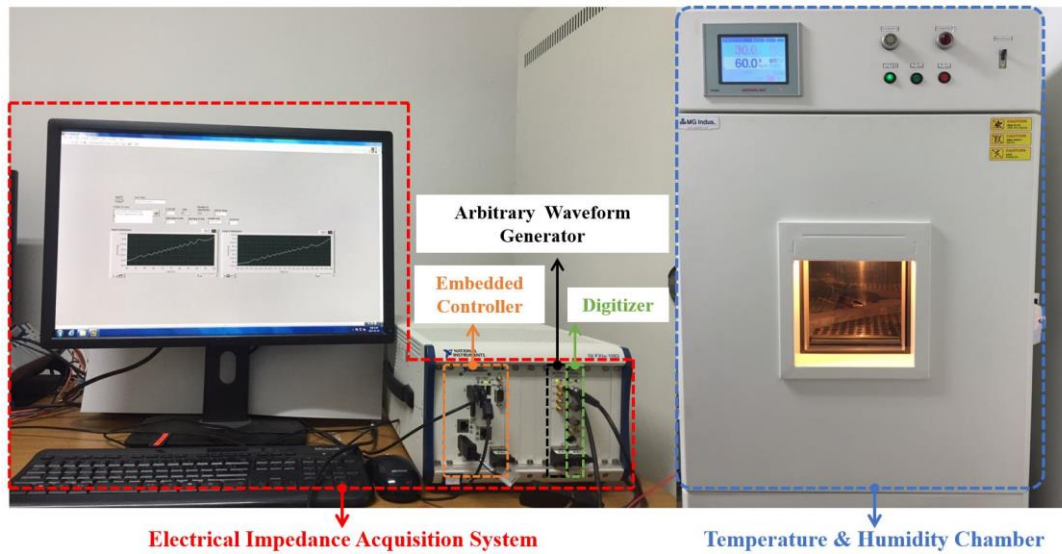


Fig. 4 Test setup for temperature and humidity variation effects

Table 3 Temperature and humidity variation test conditions

Temperature test		Humidity test	
Temperature (°C)	Relative humidity (%)	Temperature (°C)	Relative humidity (%)
-10	N.A.	20	40
0	N.A.		
10	N.A.	20	60
20	60		
30	60		
40	60		80

The measured electrical impedance basically consists of resistance (R) and reactance (X) in the broadband frequency range of interest. First, the temperature variation test results are shown in Fig. 5. R decreases while X increases according to temperature rise, although the changing patterns are different depending on the driving frequency.

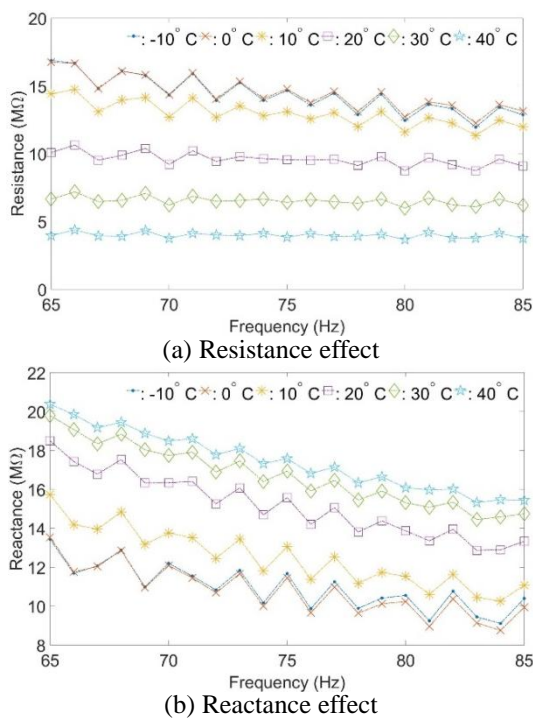


Fig. 5 Temperature effects on resistance and reactance with frequencies ranged from 65 to 85 Hz

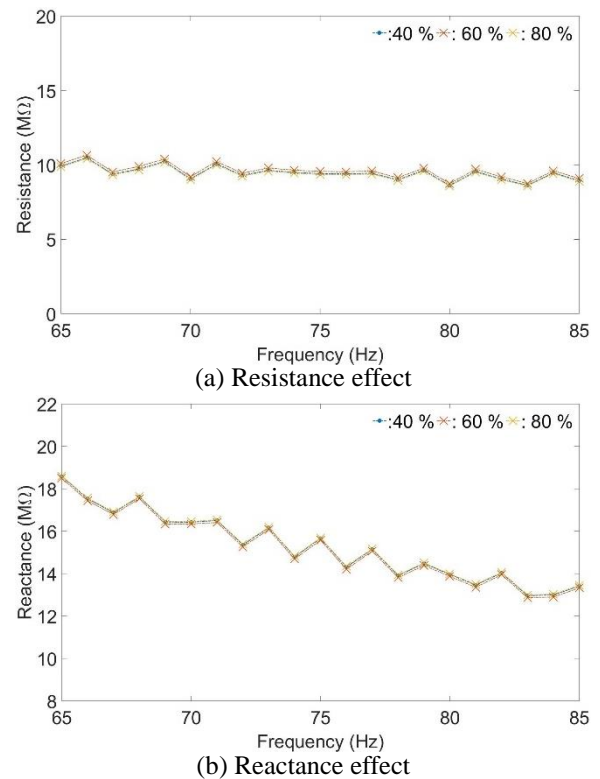


Fig. 6 Humidity effects on resistance and reactance with frequencies ranged from 65 to 85 Hz

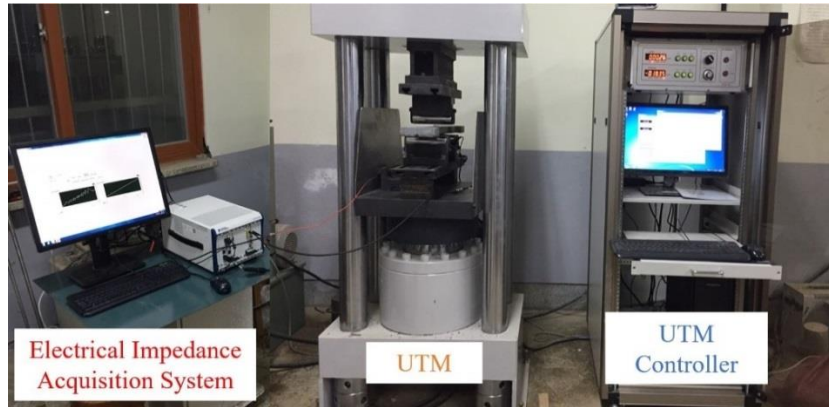


Fig. 7 Test setup for bending effects: UTM is a universal testing machine

In particular, R and X are rarely changed below 0°C , and X is less sensitive than R to temperature variation as shown in Fig. 5. Similarly, the humidity variation test results are displayed in Fig. 6. Compared to the temperature effects, the humidity effects on the impedance change can be ignorable when it comes to the humidity conditions considered in the test.

3.2 Bending load tests

Fig. 7 shows the bending test setup. Using a universal testing machine (UTM), three point-bending load tests are performed under 7°C and a relative humidity of 30%. Note that the test parameters are identical to the temperature and humidity variation tests except for particularly mentioned ones. The loading step is controlled by displacement of the UTM controller. The test displacement cases are 0, 0.5 mm, 1 mm, 2 mm, 3 mm and 4 mm.

First, the representative bottom views of the SFRC specimen without loading is shown in Fig. 8(a). After applying 0.5 mm displacement to the specimen, a closed-type crack is produced as shown in Fig. 8(b). Then, an initial open crack and multiple cracks are sequentially created by 1 mm and 2 mm displacements as displayed in Figs. 8(c) and 8(d), respectively. During the loading tests, the UTM controller continuously records the corresponding force-displacement data as shown in Fig. 9. The closed-type crack is initiated in the elastic region, meaning that it can be restored. However, the initial open crack produced beyond the yielding point and the multiple cracks at almost fracture range cannot be returned to the original condition.

Fig. 10 shows the corresponding impedance response to each loading step. R and X are minutely changed by changing loading conditions compared to the temperature variation effect displayed in Fig. 5. When the closed-type crack is initiated, R slightly decreases. However, R inversely increases after the initial open crack is created. Such tendency is retained as the crack widths are gradually expanded as shown in Fig. 10(a). The phenomenon in the case of a closed-type crack can be physically explained in that the fibers in SFRC serve as bridges for connecting electricity called as the bridge effect. The reinforced fibers inside the matrix is momentarily exposed to air at the initial

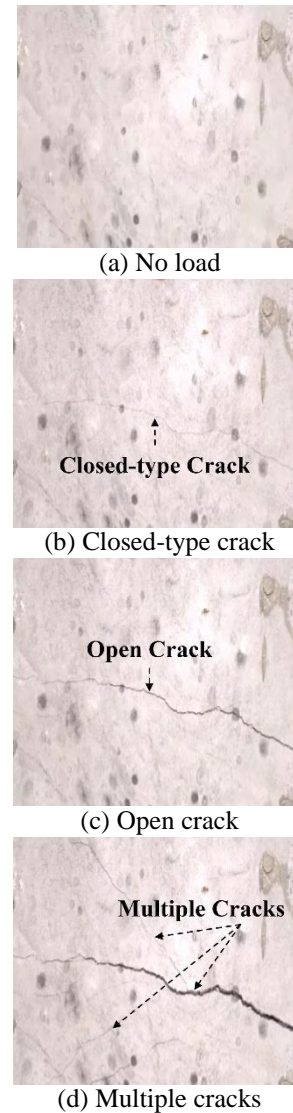


Fig. 8 The representative bottom views of the SFRC specimen under loading

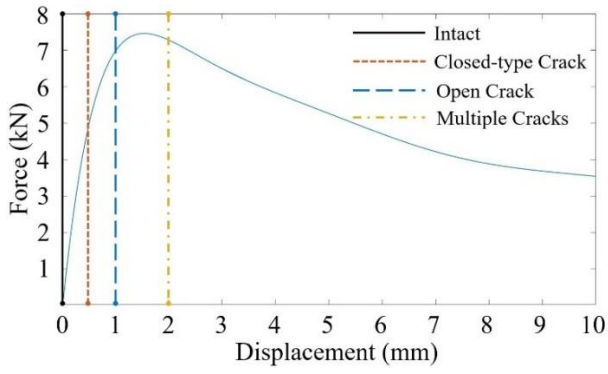


Fig. 9 Force-displacement curve and the corresponding crack generation

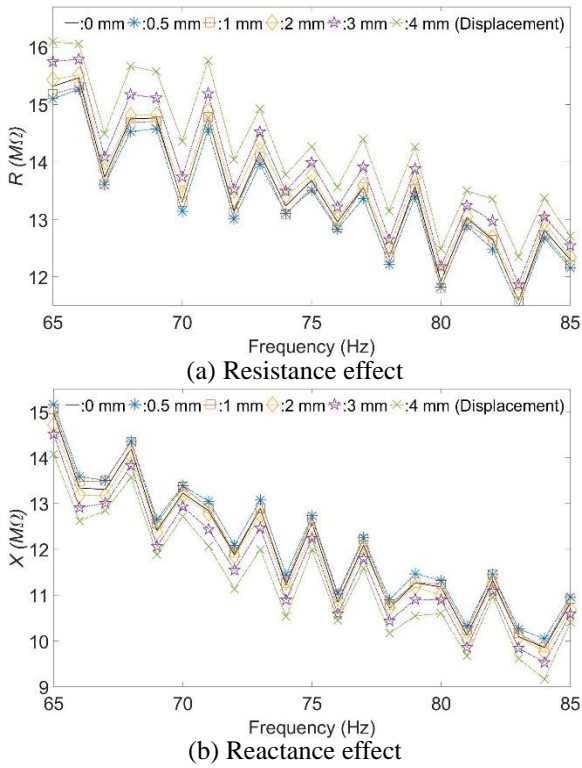


Fig. 10 Bending load effects on resistance and reactance

cracking state, resulting in the temporary R decrease. Once the crack width is more expanded, the connected bridge effect gradually diminished due to fiber separation. On the other hand, X increases due to the bridge effect while it is getting smaller as the bridge effect diminishes. Although R and X reveal the opposite changing tendency, crack initiation and expansion effects caused by the bridge effect and fiber separation can be clearly observed in Fig. 10.

4. Crack detection algorithm

Fig. 11 describes the overall procedure of a crack detection algorithm. The details of each step are as follows.

Step 1: Collect baseline data sets at various temperature conditions: Baseline data sets including R , X and the corresponding temperature are collected at various temperature conditions using the proposed electrical impedance acquisition system. It is assumed that the baseline data sets are collected from the pristine condition of a target structure. Then, the baseline phase signals (ϕ_j) are computed using R_j and X_j at each temperature condition.

$$\phi_j = \tan^{-1} \frac{X_j}{R_j} \quad (2)$$

where the subscript j denotes a certain temperature condition.

Step 2: Measure a test data set at a specific temperature: The test data set containing R , X and temperature is measured at a specific temperature condition. Once the test data set is acquired, the corresponding test phase signal (ϕ_t) is similarly calculated as Eq. (2). Here, the phase information implies the changing features of R and X .

Step 3: Select the two closest baseline data sets to the test data sets using the test temperature condition: Since the temperature information are known, the two closest baseline phase signals (ϕ_{j1}, ϕ_{j2}) to the test temperature (t) can be selected.

Step 4: Reconstruct the baseline phase signal: Using the two selected baseline phase signals, a new phase signal can be constructed by assuming the linear relationship between phase and temperature variations within the temperature interval used in the baseline data collection.

$$\phi'_t = \frac{\phi_{j1}|t - j2| + \phi_{j2}|t - j1|}{|j1 - j2|} \quad (3)$$

where ϕ'_t is the reconstructed phase signal at the test temperature. $j1$ and $j2$ are the two closest temperature values to t . The difference between ϕ_t and ϕ'_t may be different depending on temperature interval used when baseline data sets are collected. Since the baseline data sets cannot be gathered at all continuous temperature conditions, the discrepancy between ϕ_t and ϕ'_t is inevitable.

Step 5: Compute a damage index and threshold: A damage index (DI) is computed using ϕ_t and ϕ'_t

$$DI = \sqrt{\frac{\int_{sf}^{ef} (\phi_t - \phi'_t)^2 df}{\int_{sf}^{ef} (\phi'_t)^2 df}} \quad (4)$$

where sf and ef represent the start and end frequencies. In case of the intact test data sets, DI has only reconstruction and measurement errors, used for a threshold (TR) value in this study. The errors can be minimized by increasing the temperature resolution of baseline collection. On the other hand, the crack-induced feature is straightforwardly reflected in DI.

Step 6: Decision making: Once DI and TR are calculated, the SFRCs' condition can be evaluated. For example, when calculated DI is larger than TR, it is damaged condition. If not, it is undamaged condition.

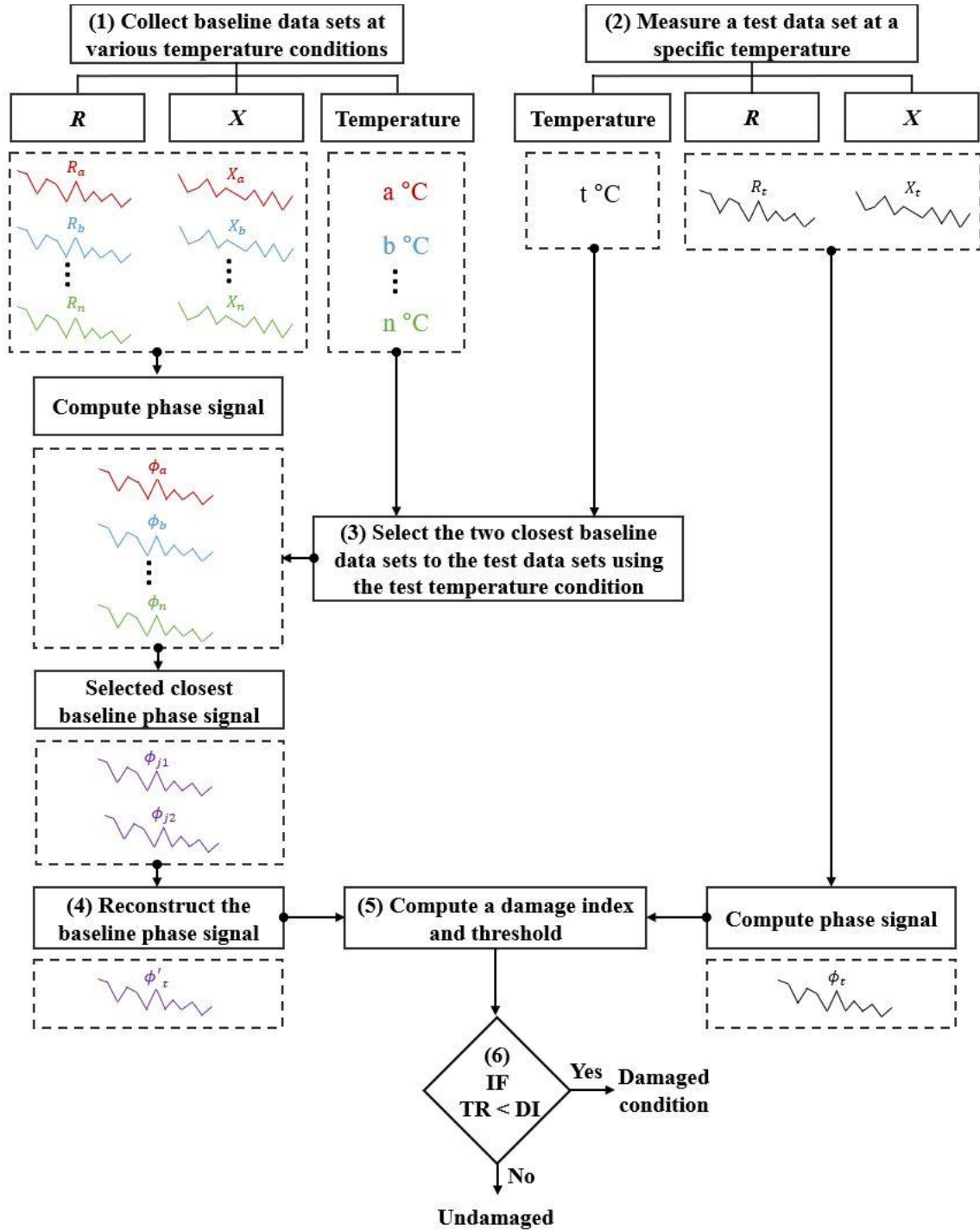


Fig. 11 Overall procedure of a crack detection algorithm: TR and DI represent threshold and damage indices

The temperature variation and bending load test data described in Section 3 are used for examining the algorithm performance. The temperature variation test data obtained at -10°C , 0°C , 10°C , 20°C , 30°C , and 40°C considered as normal operation temperature ranges of infrastructures are used as the baseline data sets. Then, the bending load test data sets obtained at 7°C is used as the test data sets. Once ϕ_j and ϕ_7 are computed by Eq. (2), ϕ'_7 can be obtained using ϕ_0 and ϕ_{10} . This calculation is repeated for each loading steps from 0 to 4 mm.

Fig. 12 shows the phase variation tendency. As expected, the discrepancy between ϕ_7 of no loading case and ϕ'_7 can be observed because the temperature interval of baseline data measurement is 10°C which is not ignorable. Again, this discrepancy physically means nothing but the reconstruction and measurement errors, acting as the threshold value, presented in the red dotted line in Fig. 13. Then, ϕ_7 corresponding to the 0.5 mm loading case increases compared to ϕ'_7 .

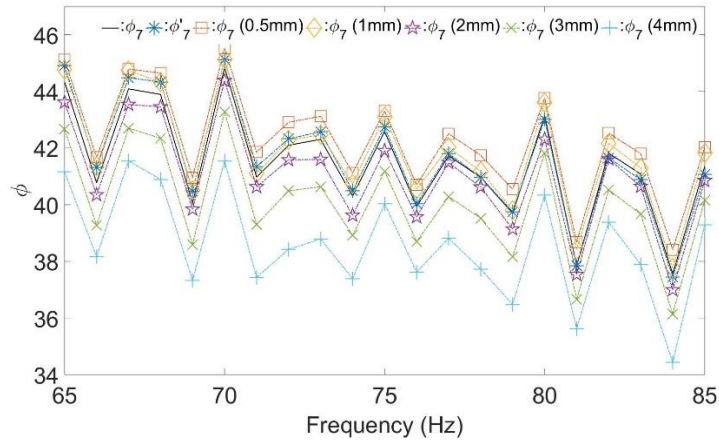


Fig. 12 Phase variation at 7°C

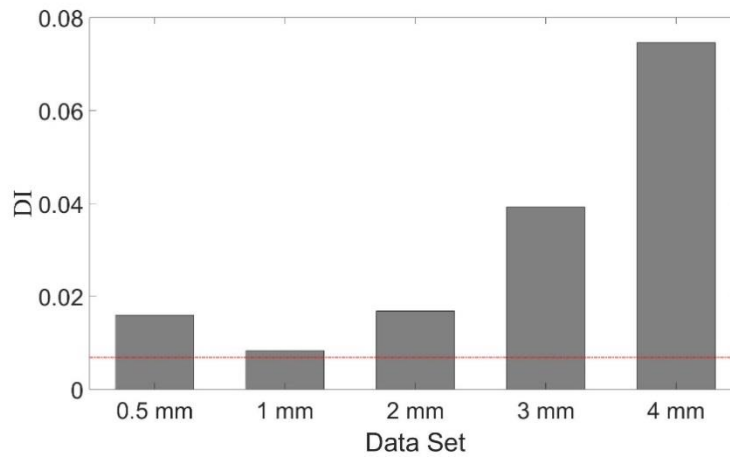


Fig. 13 Test results of the crack detection algorithm

From the 1 mm to 4 mm loading cases, inversely the ϕ_7 values decrease. Although the discrepancy between ϕ_7 of the 1 mm loading case and ϕ'_7 is the smallest among the investigated loading cases, it is still larger than the error-caused discrepancy. It can be inferred that the crack detectability depends on the error-caused discrepancy, and smaller temperature interval of baseline data collection can enhance crack detectability.

Based on the computed data, DI's are calculated using Eq. (4) and summarized in Fig. 13. It can be observed that DI's of all crack cases exceed the threshold value, meaning that the proposed algorithm successfully detects early cracks without false alarms. One interesting fact to see here is that DI of the closed-type crack corresponding to the 0.5 mm loading case is larger than the initial open crack one. The reason why DI of the 0.5 mm case is larger than the 1 mm case one is that the proposed technique is sensitive to even closed type crack (0.5 mm case) due to the bridge effect. Also, DI's of other open crack cases remarkably increase due to the subsequent fiber separation. Therefore, it can be concluded that the proposed technique is able to detect closed-type early crack as well as open-type cracks.

5. Conclusions

This paper proposes an early crack detection technique using steel fiber-reinforced concrete (SFRC)-based self-sensing electrical impedance. Since SFRC can be used as a sensor itself as well as a structural member of infrastructures, it can be effectively used for structural hot spot monitoring. For the structural health monitoring purpose using SFRC, an instantaneous electrical impedance measurement system and the corresponding crack detection algorithm are developed and experimentally validated. In particular, temperature and humidity variation effects are thoroughly investigated, because the electrical impedance is typically altered by environmental variation effects, especially temperature changes. Although the validation test results reveal that even closed-type early crack is successfully detected under certain temperature conditions, it is important to cover a wide range of temperature conditions with a small temperature increment to minimize false alarms and maximize crack detectability.

As a follow-up study, a machine learning or deep learning-based crack detection algorithm is now being developed for fully automated making-decision. Moreover, crack localization will be tested through multi-channel

sensing in a real scale concrete structures. Furthermore, the applicability or detectability to various damage types such as corrosion, spalling and etc. should be investigated before its practical usage, although its environmental effects have been investigated in this study. It is expected that the proposed technique can be practically used for monitoring various concrete structures such as building, bridge, pipe, nuclear power plant and so on.

Acknowledgments

This research was supported by a grant (16CTAP-C114934-01) from the Construction Technology Research Program, which is funded by the Ministry of Land, Infrastructure and Transport of the Korean government

References

- Aggelis, D.G., Kordatos, E.Z., Soulioti, D.V. and Matikas, T.E. (2010), "Combined use of thermography and ultrasound for the characterization of subsurface cracks in concrete", *Constr. Build. Mater.*, **24**(10), 1888-1897.
- An, Y.K., Kim, J.M. and Sohn, H. (2014), "Laser lock-in thermography for detection of surface-breaking fatigue cracks on uncoated steel structures", *NDT&E Int.*, **65**, 54-63.
- An, Y.K. and Sohn, H. (2012), "Integrated impedance and guided wave based damage detection", *Mech. Syst. Signal Pr.*, **28**, 50-62.
- An, Y.K., Lim, H.J., Kim, M.K., Yan, J.Y., Sohn, H. and Lee, C.G. (2014), "Application of local reference-free damage detection techniques to in-situ bridges", *J. Struct. Eng.-ASCE*, **140**(3).
- Arslan, M.H. and Korkmaz, H.H. (2007), "What is to be learned from damage and failure of reinforced concrete structures during recent earthquakes in Turkey?", *Eng. Fail. Anal.*, **14**(1), 1-22.
- Arun, N. and Subramaniam, K.V.L. (2016), "Experimental evaluation of load-induced damage in concrete from distributed microcracks to localized cracking on electro-mechanical impedance response of bonded PZT", *Constr. Build. Mater.*, **105**, 536-544.
- Azhari, F. and Banthia, N. (2012), "Cement-based sensors with carbon fibers and carbon nanotubes for piezoresistive sensing", *Cement Concrete Comp.*, **34**(7), 866-873.
- Bae, B.I., Chung, J.H., Choi, H.K., Jung, H.S. and Choi, C.S. (2018), "Experimental study on the cyclic behavior of steel fiber reinforced high strength concrete columns and evaluation of shear strength", *Eng. Struct.*, **157**, 250-267.
- Baoguo, H., Kun, Z., Xun, Y., Eil, K. and Jinping, O. (2012), "Electrical characteristics and pressure-sensitive response measurements of carboxyl MWNT/cement composites", *Cement Concrete Comp.*, **34**(6), 794-800.
- Chalioris, C.E., Karayannis, C.G., Angeli, G.M., Papadopoulos, N.A., Favvata, M.J. and Providakis, C.P. (2016), "Applications of smart piezoelectric materials in a wireless admittance monitoring system (WIAMS) to structures-tests in RC elements", *Case Studies in Constr. Mater.*, **5**, 1-18.
- Chalioris, C.E., Papadopoulos, N.A., Angeli, G.M., Karayannis, C.G., Liolios, A.A. and Providakis, C.P. (2015), "Damage evaluation in shear-critical reinforced concrete beam using piezoelectric transducers as smart aggregates", *Open Eng.*, **5**(1), 373-384.
- Cheng, C.C., Cheng, T.M. and Chiang, H.H. (2008), "Defect detection of concrete structures using both infrared thermography and elastic waves", *Autom. Constr.*, **18**(1), 87-92.
- Hou, T.C. and Lynch, J.P. (2005), "Conductivity-based strain monitoring and damage characterization of fiber reinforced cementitious structural components", *Proceedings of the SPIE 12th Annual International Symposium on Smart Structures and Materials*, California, USA, May
- Jahanshahi, M.R., Masri, S.F., Padgett, C.W. and Sukhatme, G.S. (2013), "An innovative methodology for detection and quantification of cracks through incorporation of depth perception", *Machine Vision Appl.*, **24**(2), 227-241.
- Jianming, G., Wei, S. and Keiji, M. (1997), "Mechanical properties of steel fiber-reinforced, high-strength, lightweight concrete", *Cement Concrete Comp.*, **19**(4), 307-313.
- Jingyao, C. and Chung, D.D.L. (2004), "Electric polarization and depolarization in cement-based materials, studied by apparent electrical resistance measurement", *Cement Concrete Res.*, **34**(3), 481-485.
- Karayannis, C.G., Voutetaki, M.E., Chalioris, C.E., Providakis, C.P. and Angeli, G.M. (2015), "Detection of flexural damage stages for RC beams using Piezoelectric sensors", *Smart Struct. Syst.*, **15**(4), 997-1018.
- Kazuro, K., Hideaki, M., Isamu, O., Makoto, K., Keiichi, N., Yuichi, M. and Fumio, M. (2005), "Acoustic emission monitoring of a reinforced concrete structure by applying new fiber-optic sensors", *Smart Mater. Struct.*, **14**(3), 52-59.
- Konsta-Gdoutos, M.S. and Aza, C.A. (2014), "Self sensing carbon nanotube (CNT) and nanofiber (CNF) cementitious composites for real time damage assessment in smart structures", *Cement Concrete Comp.*, **53**, 162-169.
- Lecompte, D., Vantomme, J. and Sol, H. (2006), "Crack detection in a concrete beam using two different camera techniques", *Struct. Health Monit.*, **5**(1), 59-68.
- Luo, J.L., Duan, Z.D., Zhao, T.J. and Li, Q.Y. (2011), "Self-sensing property of cementitious nanocomposites hybrid with nanophase carbon nanotube and carbon black", *Adv. Mater. Res.*, **143-144**, 644-647.
- Neild, S.A., Williams, M.S. and McFadden, P.D. (2005), "Development of a vibrating wire strain gauge for measuring small strains in concrete beams", *Strain*, **41**(1), 3-9.
- Providakis, C. and Liarakos, E. (2011), "T-WiEYE: An early-age concrete strength development monitoring and miniaturized wireless impedance sensing system", *Procedia Eng.*, **10**, 484-489.
- Qiao, G., Guo, B., Li, Z., Ou, J. and He, Z. (2017), "Corrosion behavior of a steel bar embedded in a cement-based conductive composite", **134**, 388-396.
- Robin, W. (2013), *Failures in Concrete Structures Case Studies in Reinforced and Prestressed Concrete*, CRC Press, Miami, FL, USA.
- Simon, A., Courtois, A., Clauzon, T., Coustabeau, E. and Vinit, S. (2015), "Long-term measurement of strain in concrete: durability and accuracy of embedded vibrating wire strain gauges", *Smart Monitoring, Assessment and Rehabilitation of Civil Structures*, Antalya, Turkey, September.
- Suraj, N.K. and Shruti, R.G. (2016), "PZT based smart aggregate for unified health monitoring of RC structures", *Open J. Civil Eng.*, **6**(1), 42-49.
- Teomete, E. (2015), "Measurement of crack length sensitivity and strain gage factor of carbon fiber reinforced cement matrix composites", *Measurement*, **74**, 21-30.
- Vaidya, S. and Allouche, E.N. (2011), "Experimental evaluation of electrical conductivity of carbon fiber reinforced fly-ash based geopolymer", *Smart Struct. Syst.*, **7**(1), 27-40.
- Verstrynge, E., Pfeiffer, H. and Wevers, M. (2014), "A novel technique for acoustic emission monitoring in civil structures with global fiber optic sensors", *Smart Mater. Struct.*, **23**(6), 1-9.

- Wang, D., Song, H. and Zhu, H. (2013), "Numerical and experimental studies on damage detection of a concrete beam based on PZT admittance and correlation coefficient", *Constr. Build. Mater.*, **49**, 564-574.
- Xu, D., Cheng, X., Huang, S. and Jiang, M. (2010), "Identifying technology for structural damage based on the impedance analysis of piezoelectric sensor", *Constr. Build. Mater.*, **24**(12), 2522-2527.
- Xuli, F., Erming, M., Chung, D.D.L. and Anderson, W.A. (1997), "Self-monitoring in carbon fiber reinforced mortar by reactance measurement", *Cement Concrete Res.*, **27**(6), 845-852.
- Yan, S., Ma, H., Li, P., Song, G. and Wu, J. (2017), "Development and application of a structural health monitoring system based on wireless smart aggregates", *Sensors*, **17**(7), 1641.
- Yang, J.Y., Hwang, S.K., An, Y.K., Lee, K.H. and Sohn, H. (2016), "Multi-spot laser lock-in thermography for real-time imaging of cracks in semiconductor chips during a manufacturing process", *J. Mater. Process. Technol.*, **229**, 94-101.
- Yanowen, Y., Yugang, H. and Yong, L. (2008), "Sensitivity of PZT impedance sensors for damage detection of concrete structures", *Sensors*, **8**(1), 327-346.
- Yoo, D.Y., Yoon, Y.S. and Banthia, N. (2015), "Flexural response of steel-fiber-reinforced concrete beams: Effects of strength, fiber content, and strain-rate", *Cement Concrete Comp.*, **64**, 84-92.